

Old Pacific Crust Near Hawaii: A Seismic View

DENNIS A. LINDWALL¹

Hawaii Institute of Geophysics, University of Hawaii, Honolulu

An expanding spread profile (ESP) over 80 Ma Pacific Ocean crust near Hawaii was modeled with a one-dimensional solution for travel times, relative amplitudes, and sometimes frequency content. The resulting profiles of compressional and shear wave velocities and Poisson's ratio are similar to those determined by other ocean crustal studies except that the shear wave Q in the sediments is very low (10) and some unusual high-frequency, high-phase-velocity arrivals require a laminated structure within the mid-crustal section at about 3 km below the base of the sediment. The laminations are probably alternating layers of gabbro and ultramafic cumulates. The cumulates may be fractionation products from an upper level magma chamber that was present at the time of crustal formation. Reflections which may correspond to these laminations have been observed in reflection records both near this ESP and in the North Atlantic. Comparison of different ophiolite models for ocean crust reveal that the most commonly used velocity-lithology model is probably in error for the pillow and dike basalts, resulting in an interpretation of overly thick layers in previous studies of refraction lines. The preferred interpretation is that the average total thickness of the pillow and dike sequences is between 1.0 and 1.5 km.

INTRODUCTION

This paper describes and discusses the detailed modeling of the seismic structure of oceanic crust in the vicinity of the Hawaiian Islands. The data consist of one expanding spread profile (ESP 1) and four sonobuoy refraction lines. ESP 1 is located about 300 km south-southwest of Oahu, Hawaii (Figure 1) on the flexural arch from the Hawaiian ridge where the flexural stress is believed to be nearly zero [Watts *et al.*, 1980; Brocher and Ten Brink, 1987]. The sonobuoys are located nearer to Oahu with sonobuoy 4 being located near the theoretical maximum dilatational stress [Watts *et al.*, 1980; Brocher and Ten Brink, 1987]. Sonobuoys 7 and 10 are located over crust of intermediate dilatational stress, and sonobuoy 9 is very close to ESP 1 (Figure 1). The emphasis of this paper is on ESP 1; the travel time models of the sonobuoys are used mostly as supporting evidence for the model developed for ESP 1. My goal was to fit all the features that are plainly visible in the ESP data by forward modeling with ray-traced and reflectivity synthetic seismograms. The parameters that could be varied in the model were compressional and shear wave velocity V_p and V_s , density, and compressional and shear attenuation (Q_p and Q_s), all as functions of depth only.

Brocher and Ten Brink [1987] and Ten Brink and Brocher [1987, 1988] previously discussed and modeled all of the data described in this paper using travel time fits and WKBJ synthetics. My model includes some complex structures in the mid crust and the Moho transition, a low-velocity zone, a shear velocity and Poisson's ratio structure, and provides a few constraints on Q for the uppermost part of the model, none of which were obtained by Brocher and Ten Brink [1987] or Ten Brink and Brocher [1987, 1988].

¹Now at Naval Oceanographic and Atmospheric Research Laboratory, Stennis Space Center, Mississippi.

Copyright 1991 by the American Geophysical Union.

Paper number 91JB00149.
0148-0227/91/91JB-00149\$05.00

Following the development of my model for ESP 1, I made a lithological interpretation of it using ophiolite and oceanic borehole data. The most commonly used data for this type of interpretation are the laboratory measurements by Salisbury and Christensen [1978] from the Bay of Islands (BOI) ophiolite. The BOI ophiolite may not, however, be representative of typical oceanic crust. Casey *et al.* [1983] believe that the BOI ophiolite was formed next to a transform fault since it has very thick dunite cumulate sequences and, in some places, very thin layered gabbro sequences. The Oman ophiolite has also been studied in detail and may be better than the BOI ophiolite for making stratigraphic interpretations [Coleman, 1981; Hopson *et al.*, 1981; Christensen and Smewing, 1981]. Here, I will compare my seismic profile with the known lithologies and velocities from both the Oman and the BOI ophiolites as well as the Point Sal ophiolite [Nichols *et al.*, 1980] and the logging results from DSDP hole 504B [Newmark *et al.*, 1985a, b; Salisbury *et al.*, 1985].

DATA

An expanding spread profile (ESP) is obtained using two ships, one towing a multichannel seismic receiver and the other shooting air guns or explosives. The ships move apart at the same speed so that the midpoint is stationary [Stoffa and Buhl, 1979]. The resulting large-aperture ESP data are a refraction line with the effects of slightly dipping layers nearly eliminated [Green, 1938; Diebold and Stoffa, 1981].

ESP 1 was first shot using an air gun array source and then was re-shot using explosives. The air gun array was fired once per minute giving 180 m shot spacing at a ship speed of 5 knots. The total air gun volume of 31 L (1900 inches³) fired at a pressure of about 8.3 MPa (1200 psi) and a depth of 15 m gave a bubble pulse frequency of 9 Hz. The 27 kg Tovex explosive charges fired every 10 min at a depth of 80 m gave a shot spacing of 1.8 km and a bubble pulse frequency of 7 Hz. The data plots shown for ESP 1 have the air gun data at ranges less than 17 km and the explosive data at greater ranges.

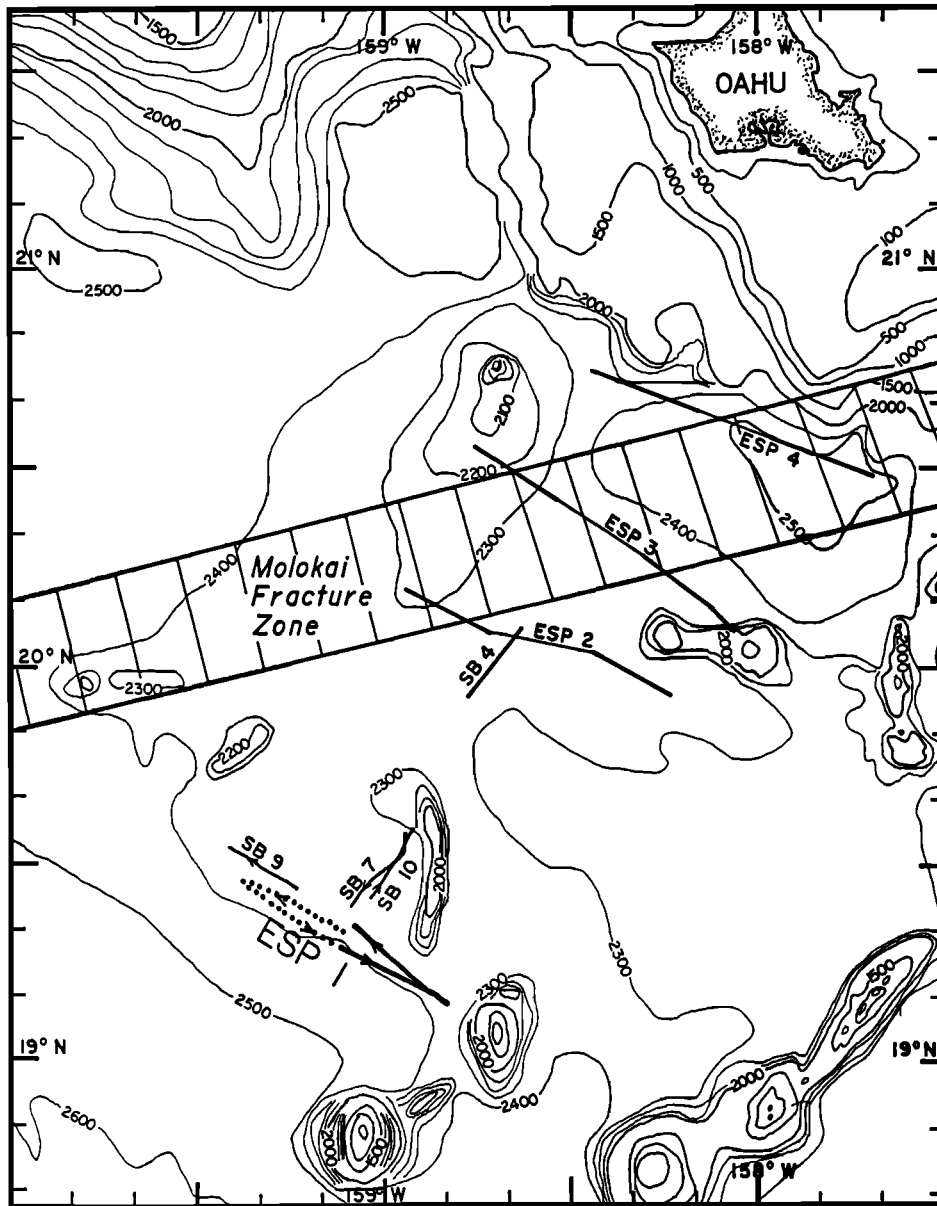


Fig. 1. Location of the expanding spread profile (ESP) and sonobuoy lines on a bathymetry (in fathoms, 1 fathom = 1.83 m) map taken from Defense Mapping Agency [1981]. ESP 1 is the main line discussed in this paper. The location of the Molokai Fracture Zone (MFZ) is from GLORIA images [Torresan *et al.*, 1989] and from Engel and Engel [1966]. For ESP 1, the track of the receiving ship was to the east and is shown by a solid line, and the shooting ship track is shown as a dashed line. For ESPs 2, 3, and 4, the receiving ship track is on the west end of the lines. The arrows on the sonobuoy lines show the ship direction.

Both ships used transit satellite navigation, and their relative range was continuously measured with Miniranger and Raydist microwave navigation systems. The shot times were measured and recorded to within 2 ms for the air guns and 30 ms for the Tovex shots. The data were recorded using the 48-channel, 3.6-km-long multichannel streamer on the R/V *Robert D. Conrad* at a sampling interval of 4 ms. The preliminary data processing involving range determination, time shifts, and binning was done at Lamont-Doherty Geological Observatory using techniques described by Stoffa *et al.* [1982], Watts *et al.* [1985], and Ten Brink and Brocher [1987].

ANALYSIS

For forward modeling of the data I used both ray-tracing synthetics and reflectivity synthetics as described by Lindwall [1988]. The dynamic ray-tracing method [Cerveny *et al.*, 1977] allows laterally varying structure, is computationally much faster, and provides ray diagrams and travel time plots that allow one to see which arrivals come from which layers. Most of the initial modeling was done with ray tracing since the ray diagrams made it easier to modify a model to better fit the data.

The ray-tracing models were further developed by forward modeling using reflectivity synthetics of the method of

Mallick and Frazer [1987, 1988]. The reflectivity synthetics are necessary for calculating the amplitudes of critically reflected arrivals and interference effects from thin layers. The reflectivity synthetics were also used to derive the V_s model, determine Q at a few depths, and to model strong multiples. The wave number range in the calculations was 0.0-0.8 s/km, and the frequency range was 0-25 Hz. The impulse response was convolved with a 15 Hz low-pass filter and source functions as described by Spudich and Orcutt [1980a, 1987].

RESULTS

The ESP 1 data are shown on the right side of Figure 2. Although no refractions are observed from the 220-m-thick sediments, V_p at the top and bottom of the sediments is 1.65 ± 0.05 and 2.2 ± 0.1 km/s, respectively, from the relative amplitudes of the reflections from the seafloor and the basement, from fitting the travel time curve of the basement reflection, and from the P to S wave conversion strength at the basement. V_s in the sediment (0.2 to 0.7 km/s at the top and bottom, respectively) is only loosely constrained by the phase velocity of the shear wave reverberations (Figure 3). Q_s in the sediment is about 10. Synthetic seismograms with an average Q_s of 20 or more in the sediments gave stronger multiple arrivals between 6 and 10 km offset and a reduced travel time of between 7 and 8 s (Figure 3). Q_p in the sediment is 50 or more, and there are no obvious P wave reverberations in the synthetics that do not appear in the data as there were for the S waves. Velocities and densities were completely modeled with high Q values. The low Q values were then tested without changing the velocities and densities.

My best fitting velocity-depth function for ESP 1 increases monotonically from the seafloor at a depth of 4.5 km, through the top of the igneous crust at 0.2 km below the seafloor, to 2.8 km below the seafloor where there are several thin, high-velocity layers (Figure 4). The laminated structure between 2.8 and 3.3 km below the seafloor is necessary to model, using reflectivity, the first arrivals seen at offsets of 18-27 km (Figures 5 and 6). These arrivals have a phase velocity of 8 km/s and a much higher frequency, about 25 Hz,

than the 7 Hz explosive source used at those ranges. A model with six layers produces stronger arrivals here than three layers but 10 layers made no further improvement.

The Moho and upper mantle produce a nearly continuous reflection from zero offset at 8 s travel time to the critical point at about 25 km offset with large amplitude between 18 and 25 km (Figures 2 and 5) and a high-velocity refraction between 25 and 65 km. A second precritical Moho reflection appears at offsets between 10 and 15 km and at reduced travel times of about 7.5 s. It can be modeled with a low-velocity reflector just below the Moho (Figure 7). These arrivals do not appear in some of the other synthetic records because they use a smoother window over the ray parameter which attenuates those arrivals. A high-velocity layer ($V_p = 9$ km/s) gives even stronger Moho reflections at 0-20 km offsets but greatly attenuates the Moho reflections at ranges beyond 30 km. Synthetics produced with multiple low-velocity layers of 20, 50, 100, and 200 m thickness did not fit the data as well as did the single, 100-m-thick layer shown.

Data and reflectivity synthetics for the best fitting model for ESP 1 are shown at lower reduction velocities in Figures 8 and 9 to give a better display of the S waves. The layer thicknesses for the V_s model were arbitrarily restricted to be the same as for the V_p model. Since values for Poisson's ratio are calculated from V_p and V_s , only those sections of the model which have a well-constrained V_s have a well-determined Poisson's ratio. S wave arrivals with a phase velocity of about 3.5 km/s are prominent at offsets from 10 km to 14 km and observable out to 27 km. Weaker S wave arrivals with a phase velocity of 4.5 km/s are visible from 17 to 40 km, particularly in the variable area record (Figure 9, top). The shear structure is well constrained at those depth ranges with an appreciable shear gradient and at the basement where the strength of the shear wave conversion depends on V_p in the sediment and V_s in the basement. These are at depths of 0.22 km below the seafloor, between 0.7 and 2.8 km below the seafloor, and greater than 5 km below the seafloor (Figure 4). At other depths the V_s model is constrained by the travel times for the arrivals from deeper layers. V_s in the laminated zone (between 2.8

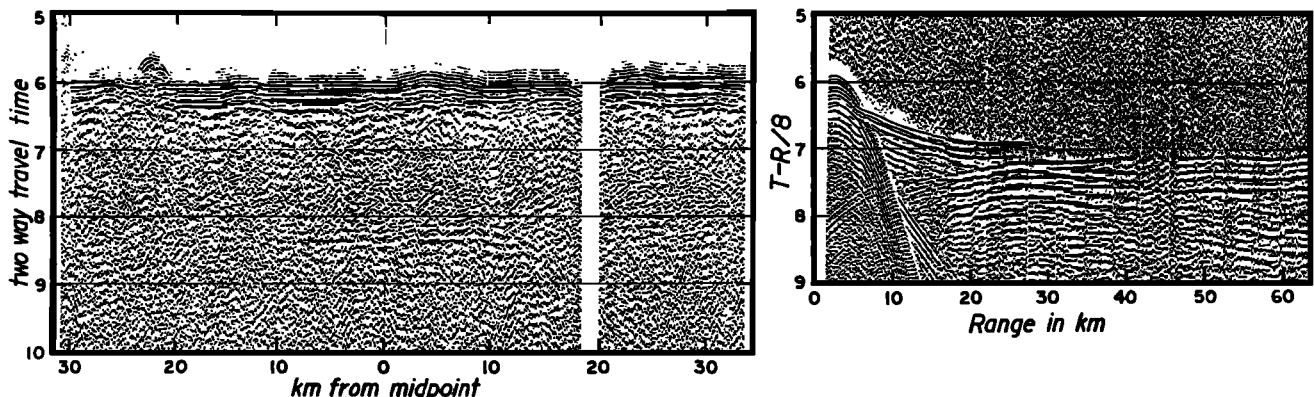


Fig. 2. The data for ESP 1 (right) plotted at a reduction velocity of 8 km/s next to the coincident reflection profile using the same time scale. Air gun sources were used for both the reflection record and the ESP record for ranges from 0 to 17 km. Beyond 17 km for the ESP line, 27 kg Tovex charges were used. The reflection Moho is just below 8 s in both records. Modeling of the high-frequency, high-phase-velocity arrivals in the ESP data at ranges between 23 and 28 km and a reduced travel time of 6.9 s gave high-velocity laminations at midcrustal levels.

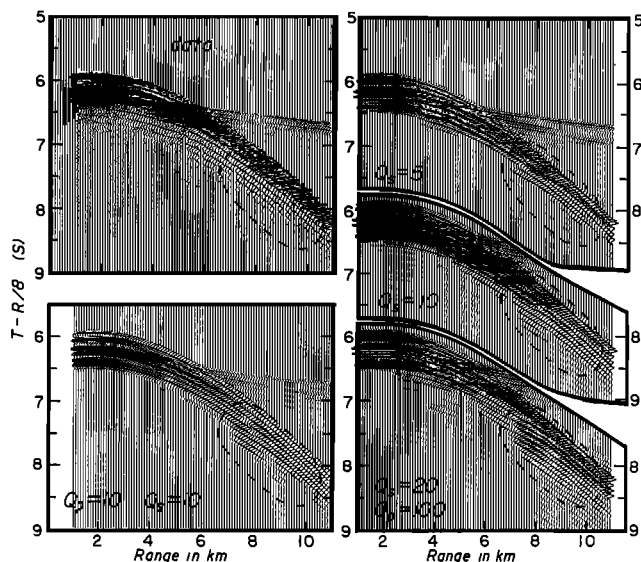


Fig. 3. A comparison of the data (top left) with synthetics using different values of Q in the sediment. The most obvious differences are in the reverberations visible at offsets between 6 and 10 km and at reduced travel times between 7 and 8.5 s. The preferred Q_p is 10. A Q_p which is too low, such as in the bottom left, gives greatly attenuated direct reflections and refractions. Q_p is 100 for the synthetics shown on the right, but any Q_p over 50 gives the same appearance.

and 3.3 km below the seafloor) was assigned a value of 4.5 km/s to give a reasonable Poisson's ratio. The shear reflection at 6.2 s reduced time at 20-30 km (Figure 9) is interpreted as the shear Moho reflection but is much stronger in the data than in the synthetics even when multiple reflectors were included in the model.

The sonobuoy solutions shown (Figure 10) are from the same data described by Brocher and Ten Brink [1987] but

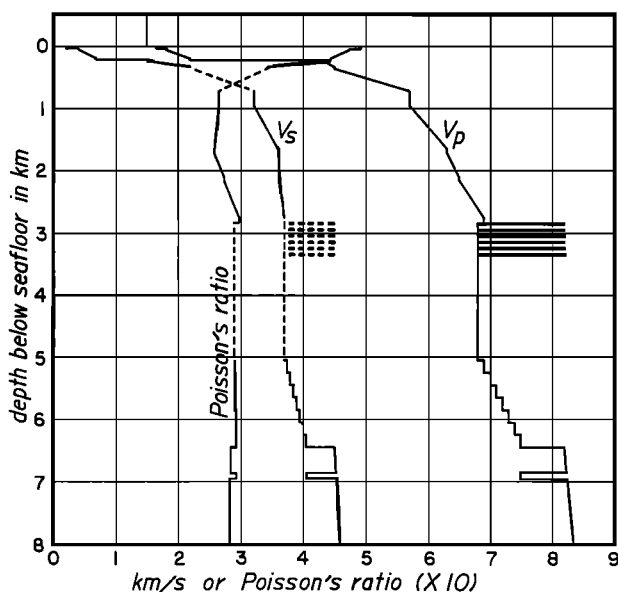


Fig. 4. Compressional wave velocity (V_p), shear wave velocity (V_s), and Poisson's ratio model which, by forward modeling, produced the best match of the reflectivity synthetics to the data (Figure 5). Poorly determined sections of the profiles are shown dashed. The depth is below the seafloor and the scale for Poisson's ratio is multiplied by 10.

were derived independently using the same technique of fitting travel times. The models for sonobuoys 7, 9, and 10 shown here are similar to each other. The most notable differences between the solution for ESP 1 and the sonobuoys are for depths between 0.5 and 1.0 km below the seafloor where both V_p and V_s for ESP 1 are up to 0.8 km/s higher than the sonobuoys. The differences below 2.8 km are due to the greater length of the ESP line and to the different modeling methods. The sonobuoy solutions by Brocher and Ten Brink [1987] for depths between 0.3 and 1.5 km below the seafloor have V_p up to 1 km/s faster and V_s up to 0.3 km/s faster than my solutions. Below 1.5 km below the seafloor our solutions are within 0.2 km/s. Sonobuoy 4 has significantly lower V_p values than the other sonobuoys at depths between 0.2 and 1.7 km below the seafloor and has no prominent shear arrivals. Since the longest sonobuoy line is only 32 km long, Moho arrivals are only seen as precritical reflections, and the depths and velocities of the Moho transition from the sonobuoy lines are therefore unreliable.

DISCUSSION

The V_p of 4.35 km/s at the top of the basement with an average gradient of 2.5 s^{-1} for the upper 500 m of the igneous crust and a V_s of 1.5 km/s with a gradient of 3 s^{-1} for the upper 150 m and 2.6 s^{-1} for the next 380 m agree with many recent seismic models for crust older than 5 Ma regardless of the location: Purdy [1983, 1987], White and Purdy [1983], Kong et al. [1985], NAT Study Group [1985], and Rohr [1987] in the North Atlantic; Spudich and Orcutt [1980a, b], Chapman and Orcutt [1985], and Kong et al. [1985] in the Pacific plate; Little and Stephen [1985], Stephen [1985] and Collins et al. [1989] in the Nazca plate; and Au and Clowes [1984] in the Juan de Fuca plate and from an ocean bottom borehole sonic log [Salisbury et al., 1985; Newmark et al., 1985a, b]. Although it is dangerous to make comparisons between oceanic crusts of different spreading rates, seismic velocity profile studies have not demonstrated major differences, so I will compare my velocity structure and its interpretation of Pacific crust to the crust of other plates.

The top of the igneous crust for the model of ESP 1 has a lower V_s than in other ocean crustal studies. Those that have S wave models have a minimum V_s of more than 2.0 km/s [Spudich and Orcutt, 1980a; Au and Clowes, 1984; NAT Study Group, 1985; Stephen, 1985; Rohr, 1987; Duennebier et al., 1987; Collins et al., 1989]. Only Purdy [1983] has a comparably slow V_s in the old crust. This difference among studies may be caused by the lack of S wave information since no shear arrivals are actually observed from the upper several hundred meters of the igneous crust. Logging measurements from DSDP hole 504B also had very low shear velocities for the upper 100 m [Newmark et al., 1985a, b; Little and Stephen, 1985]. The low V_s values modeled in ESP 1 were indirectly determined from amplitudes of S arrivals from lower layers. Since most of the P to S conversion occurred at the sediment-basement interface, a higher value for V_s resulted in much larger relative amplitudes for the shear arrivals in the synthetics than in the data. Weak P to S conversion may also be caused by a rough basement

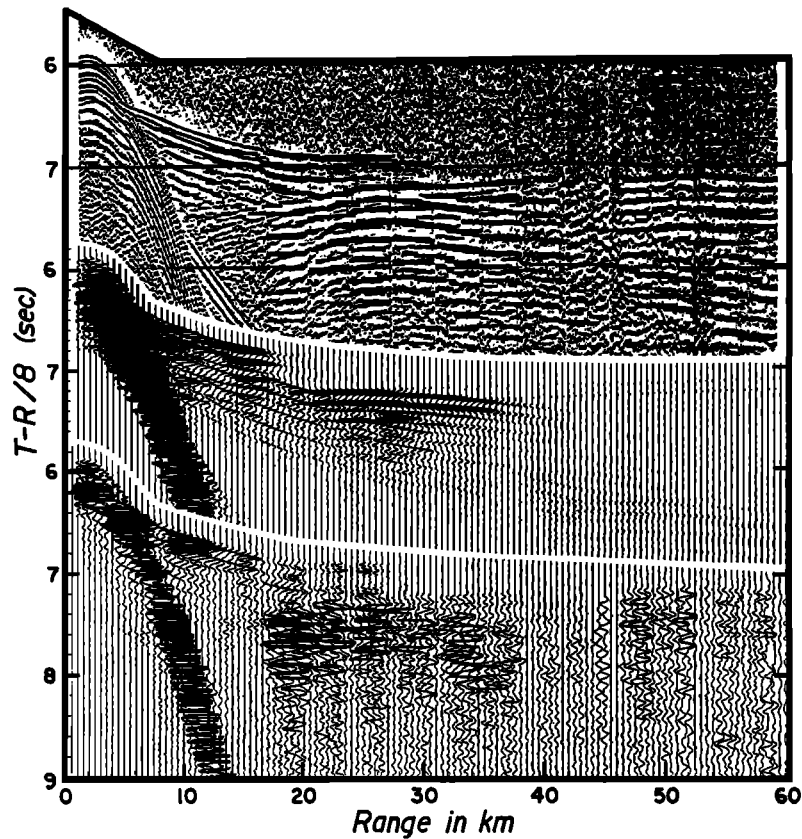
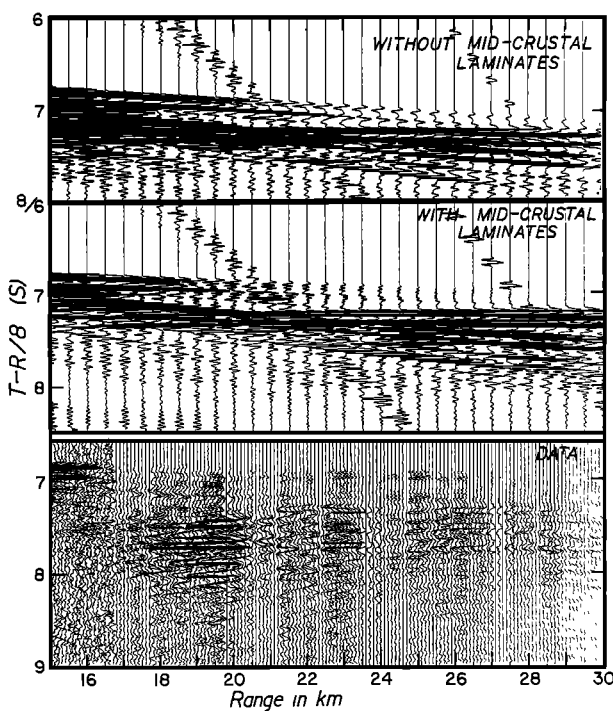


Fig. 5. Data and synthetics for ESP 1. The top section is a variable area plot of the data with 100 m trace spacing using an automatic gain filter. The bottom section is a wiggle line plot of the data with 500 m spacing (5 traces summed), and the true amplitudes are multiplied by the range. The middle section is the reflectivity synthetic with 500 m spacing between traces and the amplitude multiplied by the range. An air gun source was used at ranges less than 17 km and 27 kg Tovex charges beyond 17 km. The amplitudes of the two sections were adjusted so that they matched where they join, but uncertainties remain in the relative amplitudes since there are rapid variations in the amplitudes of the dominant arrivals near 17 km.



where the roughness is on the scale of one wavelength for S waves but is not large enough to be noticeable with P waves, roughly a range between 150 and 300 m for the sources used here.

This is the first refraction study of oceanic crust to report high-velocity laminations at midcrustal depths (2.8-3.3 km below the seafloor in Figure 4), but high-velocity caps over the underlying oceanic crustal layer 3 were described by *NAT Study Group* [1985] for 118 Ma Atlantic crust, by *Duenebier et al.* [1987] for 110 Ma Pacific crust, and by *Collins et al.* [1989] for 5.9 Ma Nazca crust. All of these models have an increased velocity gradient just above the

Fig. 6. Comparison of synthetic sections with (middle) and without (top) the laminations at 2.8-3.3 km below the seafloor (Figure 4) to the data (bottom) at an enlarged scale. The high-frequency, high-phase-velocity arrivals at a reduced travel time of 6.9 s are visible in the synthetics using the laminated model and the data. These arrivals have a frequency of about 25 Hz, while the explosive source bubble pulse is 7 Hz. The high-frequency arrivals in the synthetics have a smaller amplitude (the synthetic sections have a larger gain than the data) and a lower phase velocity than the data but have the same frequency. The low-phase velocity arrivals crossing the synthetic record section are wraparound artifacts.

TABLE 1. ESP 1 Model

Depth, km	Thickness, km	V_p , km/s	V_s , km/s	Q_p	Q_s	Density, gm/cm ³	Gradient Layers
0.00	0.01	1.5	0	5000	0	1.03	
0.01	0.005	1.5	0	5000	0	1.03	
0.015	4.485	1.5	0	5000	0	1.03	
4.50	0.04	1.65	0.4	100	10	1.2	
4.54	0.02	1.8	0.6	100	10	1.4	
4.56	0.14	1.8/2.2	0.6/0.7	100	10	1.4/1.6	7
4.70	0.02	2.2	0.7	100	10	1.6	
4.72	0.02	4.35	1.5	300	60	2.2	
4.74	0.09	4.35/4.5	1.5/2.2	300/450	60/100	2.2/2.3	6
4.83	0.02	4.5	2.2	450	100	2.3	
4.85	0.36	4.5/5.7	2.2/3.22	450/600	100/300	2.3/2.7	7
5.21	0.24	5.7	3.22	600	300	2.7	
5.45	0.70	5.7/6.3	3.22/3.6	600/800	300/400	2.7/2.9	12
6.15	0.05	6.3	3.6	800	400	2.9	
6.20	0.40	6.3/6.5	3.6/3.63	800/1000	400/500	2.9/3.0	7
6.60	0.05	6.5	3.63	1000	500	3.0	
6.65	0.60	6.5/6.9	3.63/3.7	1000	500/600	3.0	9
7.25	0.08	6.9	3.7	1000	600	3.0	
7.33	0.02	8.2	4.5	1000	1000	3.3	
7.35	0.08	6.8	3.7	1000	600	3.0	
7.43	0.02	8.2	4.5	1000	1000	3.3	
7.45	0.08	6.8	3.7	1000	600	3.0	
7.53	0.02	8.2	4.5	1000	1000	3.3	
7.55	0.08	6.8	3.7	1000	600	3.0	
7.63	0.02	8.2	4.5	1000	1000	3.3	
7.65	0.08	6.8	3.7	1000	600	3.0	
7.73	0.02	8.2	4.5	1000	1000	3.3	
7.75	0.08	6.8	3.7	1000	600	3.0	
7.83	0.02	8.2	4.5	1000	1000	3.3	
7.85	1.7	6.8	3.7	1000	600	3.0	
9.55	1.4	6.9/7.5	3.75/4.05	1000	600/750	3.0	7
10.95	0.2	8.2	4.50	1000	1000	3.3	
11.15	0.2	8.225	4.51	1000	1000	3.3	
11.35	0.1	7.5	4.05	1000	1000	3.0	
11.45	2.6	8.25/8.5	4.52/4.7	1000	1000	3.3	13
14.05	5.0	8.5	4.7	1000	1000	3.3	

Gradients are approximated with zones of many thin layers. The velocities, Q_s , and densities for the top and bottom layers in gradient zones are shown above with a "/" between them. A linear interpolation is used for the values in the intermediate layers.

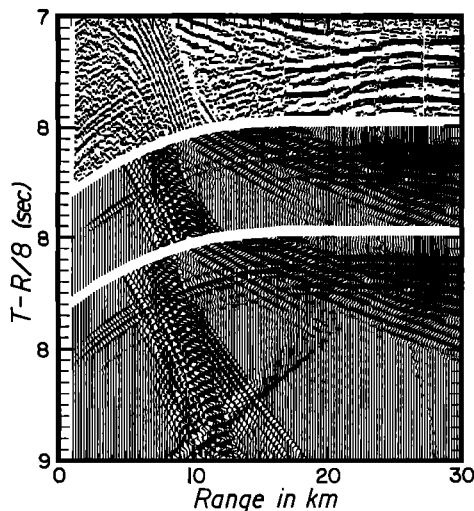


Fig. 7. Data (top) and reflectivity synthetics showing the precritical Moho reflection without (middle) and with (bottom) the sub-Moho, low-velocity zone shown in Figure 4. There is a source change in the data at 17 km from air guns to 27 kg Tovex charges, while the synthetics used a simulated air gun source at all ranges.

high-velocity caps. The high-velocity layers in the ESP 1 model are much thinner, only 20 m thick, but have a poorly determined velocity. The frequency content of these arrivals requires that they be about 100 m apart. The arrivals in the synthetics from these layers do not fit the data well, probably because the actual layers are very irregular. The reflectivity synthetics assume that they are horizontally stratified. These layers may be analogous to the lower crustal reflections seen in multichannel profiles in the North Atlantic [Mutter and NAT Study Group 1985; McCarthy and Mutter, 1986; McCarthy et al., 1988] or to the more diffuse and intermittent intracrustal reflections which were observed only about 70 km to the east of ESP 1 [Ten Brink and Brocher, 1988]. The reflectors described by both McCarthy et al. [1988] and Ten Brink and Brocher [1988] are dipping 20°-40° which, if either is analogous to the layers reported here, may explain why the corresponding arrivals in the synthetics do not fit the phase velocity well. The thin, high-velocity layers may be present below 8 km depth in ESP 1 (Figure 4), but the data do not require them because the resulting arrivals would be obscured by the stronger Moho arrivals.

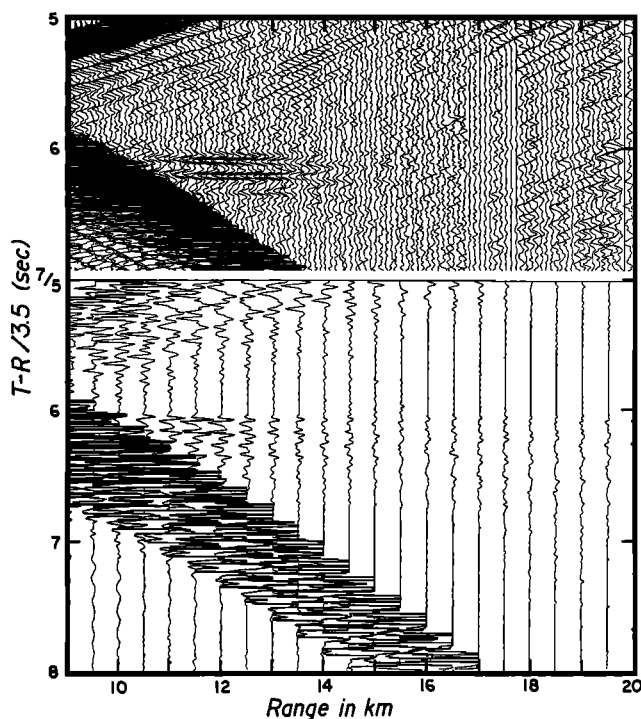


Fig. 8. Data (top) and reflectivity synthetics (bottom) plotted at a reduction velocity of 3.5 km/s to better show the slower shear arrivals which come from structure at 1-3 km below the seafloor.

The high-velocity laminations may be either ultramafic sills or ultramafic cumulates from an upper level magma chamber interbedded with slower gabbros. Ultramafic intrusions are present at nearly all levels of the crust in the Oman ophiolite [Hopson *et al.*, 1981; Nicolas *et al.*, 1988; Juteau *et al.*, 1988a, b; Reuber, 1988]. Ultramafic sills may result from high-level intrusives from off-ridge magmatism. The numerous, small seamounts near ESP 1 (Figure 1) are believed to be near-ridge in origin [Sager and Pringle, 1987], and there may be associated subsurface intrusions nearby. If the intrusions were of primitive magma, then layers of ultramafic cumulates could be formed. Another explanation is that high-velocity ultramafic layers fractionated out of a spreading center magma chamber. Ultramafic cumulates at the base of the crust are predicted by models having large spreading center magma chambers, but it is uncertain how to get them at higher levels. The shapes of spreading center magma chambers are uncertain, however, and cumulates may be deposited on any sloping or irregular sides, or the magma chambers may be very thin. McCarthy *et al.* [1988] suggested that their lower crustal reflectors may also be crustal-penetrating fault zones. Fault zones would probably have lower velocities from mylonitization and/or serpentinization than the surrounding rocks which would give much lower amplitude reflections than the critically reflecting high-velocity layers in the model presented here.

Low-velocity zones (LVZs) similar to the one below 2.8 km (Figure 4) have been reported before [Lewis and Snydman, 1977; Bunch and Kennett, 1980; Spudich and Orcutt, 1980a, NAT Study Group, 1985; Duennebier *et al.*, 1987; Collins *et al.*, 1989]. A lithological interpretation based

on ophiolite studies discussed in the next section suggests that the LVZ is a layered gabbro sequence and the 1 km above it is an isotropic gabbroic layer [Christensen, 1978; Salisbury and Christensen, 1978; Christensen and Smewing, 1981; Christensen and Salisbury, 1982].

The velocity gradient between 5 and 6.5 km below the seafloor (Figure 4) may be due to increased olivine content in the gabbro or from interbedded layers of ultramafics and gabbro with the percentage of ultramafics increasing downward. The reflections in the data at 8 s and 0 km offset (Figures 2 and 5) are from a higher-level structure than what produces the refractions with $V_p > 8$ km/s and may be from some ultramafic layers that are as much as 2 km above the residual mantle. Therefore the reflection Moho seen in reflection profiles may be from gabbro-ultramafic laminations well above the residual upper mantle [Brocher *et al.*, 1985; Collins *et al.*, 1986]. Thin ultramafic layers which are 1 or 2 km above the Moho have been reported in

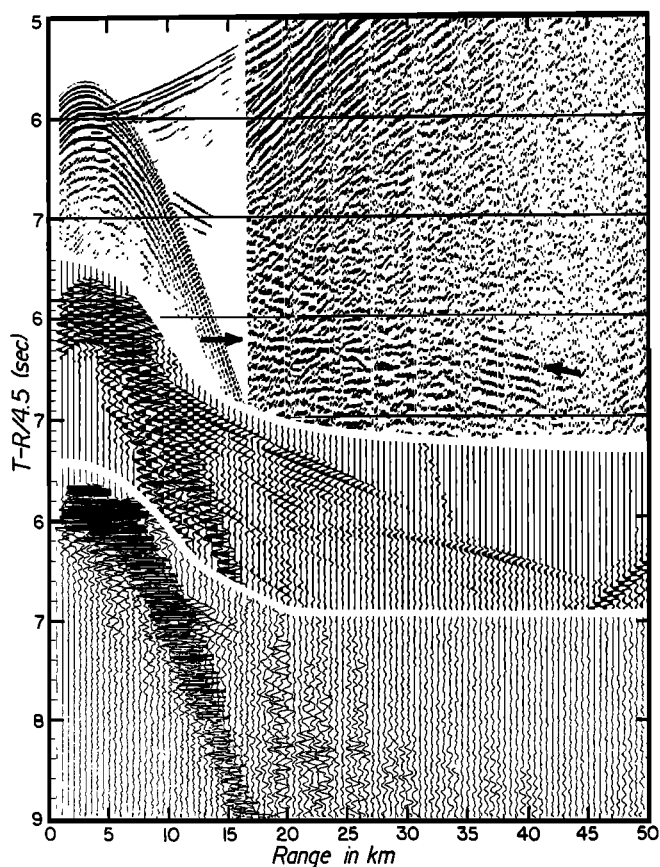


Fig. 9. Data and synthetics for ESP 1 plotted with a reduction velocity of 4.5 km/s to show all of the shear arrivals. The top section is a variable area plot of the data with 100 m spacing using an automatic gain filter. The bottom section is a wiggle line plot of the data with 500 m spacing (5 traces summed), and the true amplitudes are multiplied by the range. The middle section is the reflectivity synthetic with 500 m spacing between traces and the amplitude multiplied by the range. The slower shear arrivals (about 3.5 km/s) from the 1-3 km deep layers are visible in both the data and the synthetics out to a range of 27 km. The faster, later arrivals (about 4 km/s) from the Moho transition are visible at a reduced travel time of 8.2-8.5 s and offsets from 17 to 45 km and were strengthened by the thin low-velocity zone at 6.9 km below the seafloor.

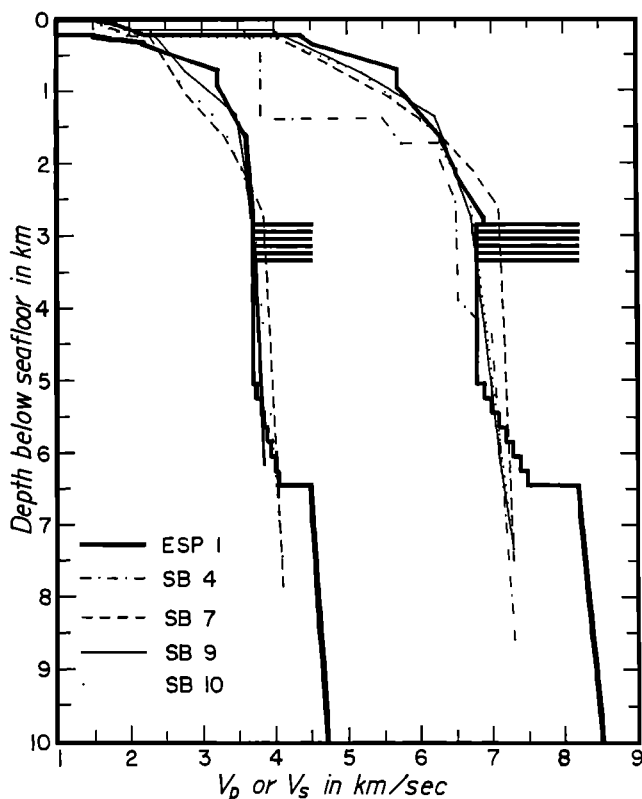


Fig. 10. Velocity-depth profiles for ESP 1 and the four sonobuoys located in Figure 1. Both P and S wave velocities are shown except for sonobuoy 4 which had no visible S wave arrivals. The sonobuoy models were derived from travel time fits. Since the maximum offsets for the sonobuoys were about 30 km, the depths to the Moho and the velocities of the upper mantle are uncertain.

the Oman ophiolite [Hopson *et al.*, 1981; Christensen and Smewing, 1981; Nicolas *et al.*, 1988; Juteau *et al.*, 1988a, b; Reuber, 1988] and in the BOI ophiolite [Salisbury and Christensen, 1978; Casey and Karson, 1981; Christensen and Salisbury, 1982; Karson *et al.*, 1984].

The variation of Poisson's ratio with depth shown in Figures 4 and 11 is consistent with previous studies (Figure 12). The upper few hundred meters of igneous crust have higher Poisson's ratios than laboratory measurements. This is probably caused by the high porosity and large-scale cracks which reduce V_s to a greater extent than V_p [Spudich and Orcutt, 1980a]. Between 0.5 and 1.45 km below the base of the sediment, Poisson's ratio is about 0.26, which is below that of almost all laboratory measurements but not as low as determined by other ocean seismic refraction experiments (Figure 12).

A very low Poisson's ratio is diagnostic of anisotropy in the vertical plane resulting from horizontal fractures [Fryer *et al.*, 1989]. The low value of 0.26 found here between depths of 0.5 and about 1.8 km below the base of the sediments almost certainly indicates horizontal fracturing. Such fracturing may extend to depths of less than 0.5 km, but at those shallow depths, Poisson's ratio is increased by the higher concentration of random cracks [Spudich and Orcutt, 1980a]. The results here agree with those of Spudich and Orcutt [1980a] but differ from Au and Clowes [1984] in that their values of V_p and V_s in the upper 3 km of igneous

crust are lower than for ESP 1 and that their zone of low Poisson's ratio (less than 0.27) is from about 1 to 3 km below the base of the sediment (Figure 12). The unusually low velocities reported by Au and Clowes [1984] may be caused by the location of their lines over the Nootka Fracture Zone.

The ESP 1 model (Figure 4), above 2.8 km below the seafloor, is very close to my sonobuoy models and to the travel time derived model for ESP 1 by Ten Brink and Brocher [1988] except for the 240-m-thick layer of constant velocity at 0.7 km. The thin, high-velocity layers between 2.8 and 3.3 km below the seafloor and the low velocities at 3-5 km below the seafloor are not in the Ten Brink and Brocher [1988] model. These differences can be attributed to my inclusion of the amplitudes and sometimes the waveforms as well as travel times in the modeling and to the fitting of the high-frequency arrivals at 18-25 km and 6.8-7.2 s reduced travel time (Figures 2 and 5).

The amplitudes in the sonobuoy records vary greatly with both range and from one record to the next. A structural study based on amplitude-derived models was not done. There is, however, one feature which is similar in the relative amplitudes of sonobuoys 7, 9, and 10, as well as ESP 1: the rapid decrease in the amplitude of the first arrival between 16 and 18 km offset. This feature is modeled in ESP 1 by the low-velocity zone below 2.8 km below the seafloor (Figure 4). A similar low-velocity zone was used by Collins *et al.* [1989] to model a similar amplitude change in sonobuoy data collected near DSDP site 504B.

Azimuthal anisotropy would appear, if present, as a systematic difference between the two perpendicular pairs of lines unless they are both oriented 45° from the principal axes. ESP 1 and sonobuoy 9 are oriented perpendicular to sonobuoys 7 and 10 (Figure 1), yet there is no apparent difference between these lines, so azimuthal anisotropy is not observed. Brocher and Ten Brink [1987] note that the flexural stress near ESP 1 should be very small so stress induced anisotropy should be unobservable.

Sonobuoy 4 differs substantially from the others shown here (Figure 10). V_p is always lower in the model for sonobuoy 4 than the other sonobuoys or ESP 1. This may be because it is located near the Molokai Fracture Zone (MFZ) (Figure 1). Lower velocities in the upper crust have been previously noted for fracture zones [Cormier *et al.*, 1984; White *et al.*, 1984], but the crust is not observed to be thinner for sonobuoy 4, perhaps because the Moho is only seen as a precritical reflection and the south end of the line, where the large offset sources were, may be south of the MFZ and over normal crust (Figure 1).

The low values for V_p in the upper crust for sonobuoy 4 along with similar results for ESPs 2, 3, and 4 and another sonobuoy adjacent to sonobuoy 4 were interpreted by Brocher and Ten Brink [1987] as being a result of extensional stress caused by flexure, but these authors were not then aware that the MFZ was located under or near those five lines. Ten Brink and Brocher [1988] interpreted the low upper crustal velocities as evidence for a thicker layer 2 in the crust to the south of the MFZ. A more likely explanation is that the low velocities are a result of the MFZ. The V_p solutions of Ten Brink and Brocher [1988] for ESP 2 and

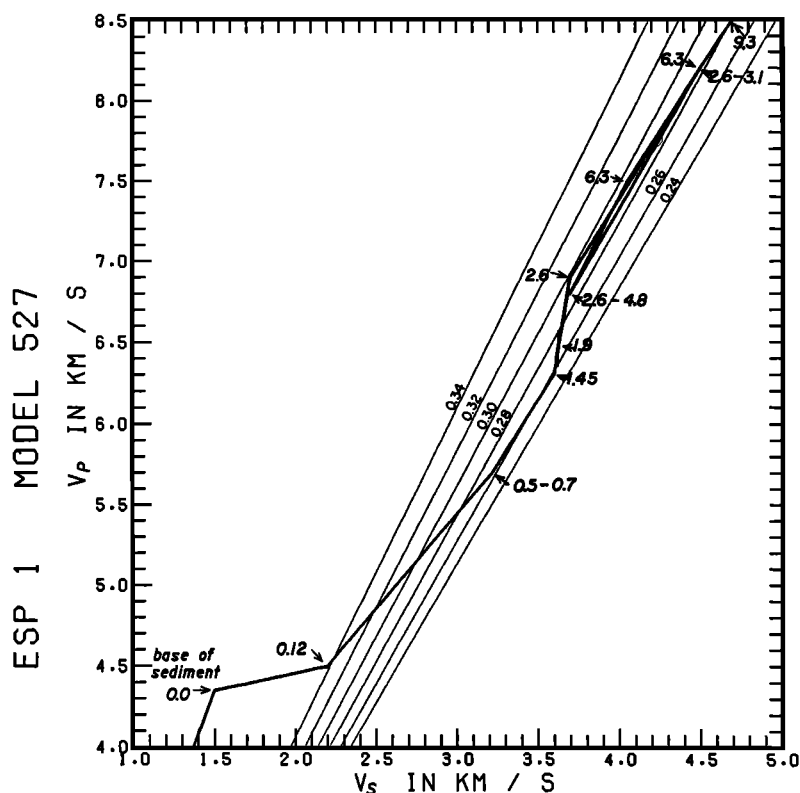


Fig. 11. V_p plotted against V_s with lines of constant Poisson's ratios (the straight, diagonal lines). The depths below the base of sediment are annotated with arrows. Between depths of 0.5 and 1.9 km the Poisson's ratio is lower than almost any laboratory measurements of ocean crustal rocks. These low values may be caused by the presence of anisotropy.

3 show a Moho that is 1-2 km deeper than for both ESP 1 and the ESPs located north of the Hawaiian islands. The model for ESP 4 by *Ten Brink and Brocher* [1987] also shows a substantially thickened crust. However, the record sections for ESPs 2, 3, and 4 show strong evidence for lateral structure in the Moho at offsets greater than 40 km where supposedly postcritical arrivals have phase velocities exceeding 20 km/s for ESP 3 and 10 km/s for ESPs 2 and 4. The Moho depths for ESPs 2 and 3 reported by *Ten Brink and Brocher* [1988] and for ESP 4 by *Ten Brink and Brocher* [1987] are probably much too deep as a result of trying to fit travel time curves and WKBJ synthetics from one-dimensional models to data collected over the complex structure of the MFZ.

LITHOLOGIC INTERPRETATION

The traditional ocean crustal layers 1, 2, and 3 were originally defined from layer cake models with thick, constant-velocity layers. These labels are of limited value in describing velocity profiles having gradients, so I have instead chosen to make a lithological interpretation of my velocity profile based on ophiolite studies. Except for a few shallow boreholes, ophiolites are the best that we have for assigning compositions to ocean crustal seismic velocity profiles.

Several field studies of ophiolites have estimated the average thicknesses of each lithological unit [*Salisbury and Christensen*, 1978; *Hopson et al.*, 1981; *Casey and Karson*, 1981; *Christensen and Smewing*, 1981; *Nehlig and Juteau*,

1988; *Juteau et al.*, 1988], and a lithological interpretation of a seismic profile could conceivably be based on the depth in the section, but I will instead use the measured velocities of samples from three ophiolites [*Salisbury and Christensen*, 1978; *Nichols et al.*, 1980; *Christensen and Smewing*, 1981] and the borehole measured velocities from DSDP site 504B [*Newmark et al.*, 1985a, b; *Salisbury et al.*, 1985]. Since this approach relies on the physical properties of the various rock types and ignores the stratigraphic thicknesses of the ophiolites from field measurements, I derived independent sequence thicknesses directly from the velocity-depth solutions.

The BOI ophiolite study of *Salisbury and Christensen* [1978] is used more often than others for making lithological interpretations of seismic profiles [e.g., *Spudich and Orcutt*, 1980a, b; *Au and Clowes*, 1984; *Bratt and Purdy*, 1984], but it has considerably higher velocities for the pillow and dike basalts than the other two ophiolites and the 504B measurements. However, using velocities that are too high for pillow and dike basalts will result in an interpretation that has overly thick pillow and dike layers. The velocity profiles of *Bratt and Purdy* [1984] and *Spudich and Orcutt* [1980a] are very similar to those presented here, and the lithological interpretations based on the BOI velocities give a thickness for the pillows and dikes of about 40% of the total crustal thickness. Using the velocities from the Oman and Point Sal ophiolites and from DSDP hole 504B gives a total thickness of from 1 to 1.3 km for the pillow and dike layers for the ESP 1 velocity profile, 1.3 km for

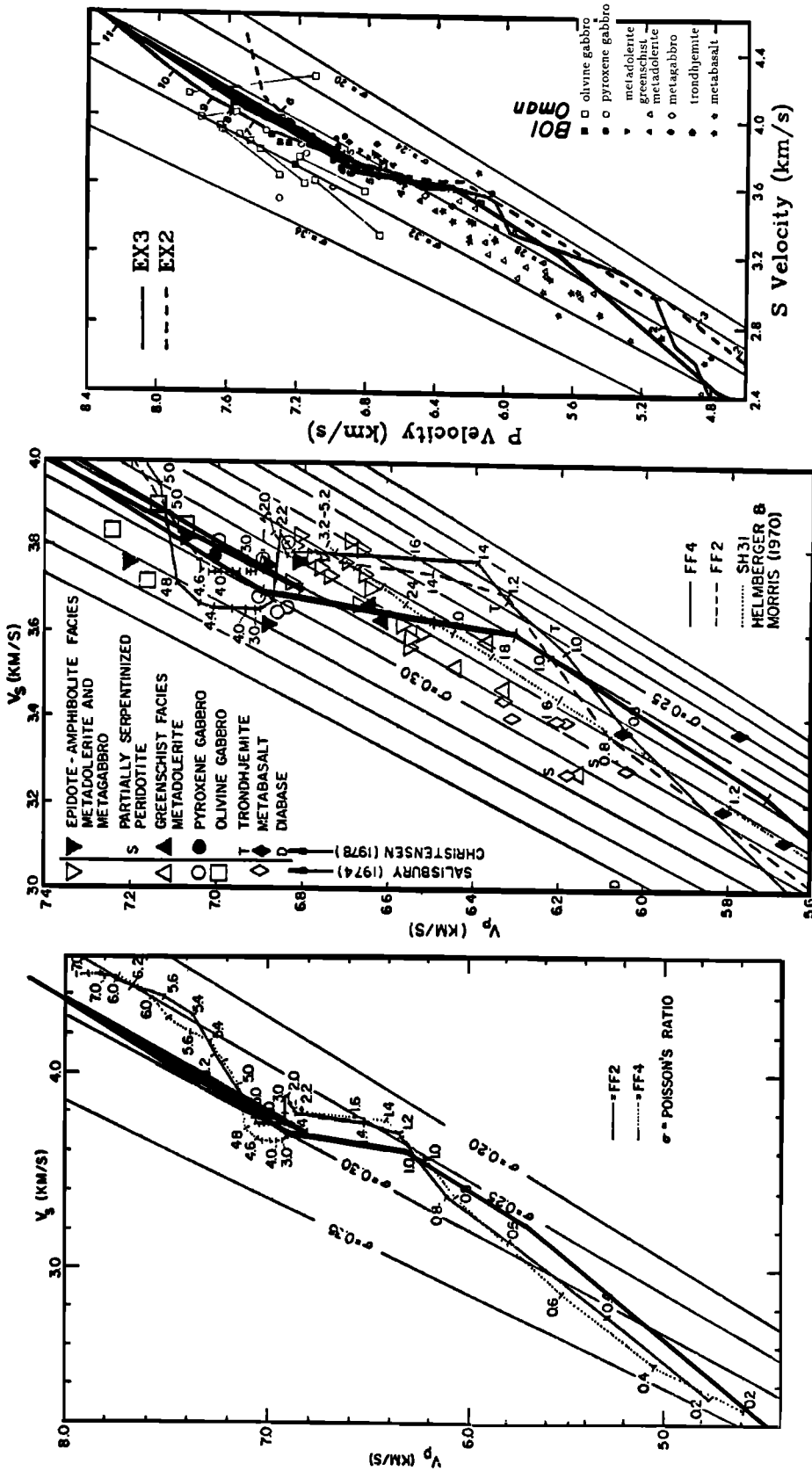


Fig. 12. Rescaled plots of Figure 11 overlain on other similar plots from Spudich and Orcutt [1980a], their Figures 19 (left) and 20 (middle), and Au and Clowes [1984], their Figure 11 (right). The lowest values for Poisson's ratio for ESP 1 are not as low as FF2 and FF4 of Spudich and Orcutt [1980a] or EX2 and EX3 of Au and Clowes [1984]. These differences may be due to real differences in the locations, different techniques (although all were modeled with reflectivity synthetics), or errors in the synthetics fitting and data collecting and processing. The middle and right plots show plotted values for samples from the Bay of Islands (BOI) and Oman ophiolites. Low values of Poisson's ratio are probably caused by the presence of anisotropy rather than a particular rock type. In general, basalts have a Poisson's ratio below 0.29 and gabbros are above 0.29, so the basalt to gabbro transition, in the absence of significant anisotropy or fracturing, can be identified as about 2 km below the base of the sediments for ESP 1. Since there is probably some anisotropy present at those depths, the basalt to gabbro transition may be several hundred meters higher.

the results of *Bratt and Purdy* [1984], and less than 1 km for those of *Spudich and Orcutt* [1980a].

Rather than relying only on the velocities from the BOI ophiolite, *Spudich and Orcutt* [1980a] argued that the pillow and dike basalt layers should have a high porosity, which raises the Poisson's ratio. Since their Poisson's ratios below 1 km are less than 0.26, requiring low porosity, they concluded that their pillow and dike layers are only 1 km thick, which is much thinner than what a comparison with just the BOI velocities would imply.

Au and Clowes [1984] made an interpretation of their velocity profiles based primarily on the BOI velocities, and although they did consider the Oman velocities, they nevertheless concluded that the pillow and dike layers had a total thickness of between 2 and 3 km for their two lines.

Using rock velocities from Oman, Point Sal, or 504B would only decrease this to 1.5-2 km. Their velocity profiles, as noted earlier, have substantially lower velocities than the great majority of ocean crustal velocity profiles, including ESP 1. This is probably because their lines were located over, or very close to, a fracture zone.

There is additional information besides the V_s and V_p values that can be used for assigning lithologies. The layers of zero velocity gradient (0.7-0.95 km, and 3.35-5.05 km below the seafloor) are certainly not regions of transition from one major division to another. The region with a Poisson's ratio of 0.26 (0.8-1.9 km below the seafloor) must have low porosity and is probably below the pillow and sheet flow layer. If the laminated zones (2.75-3.35 km and perhaps 5-6.5 km below the seafloor) are layers of cumulates,

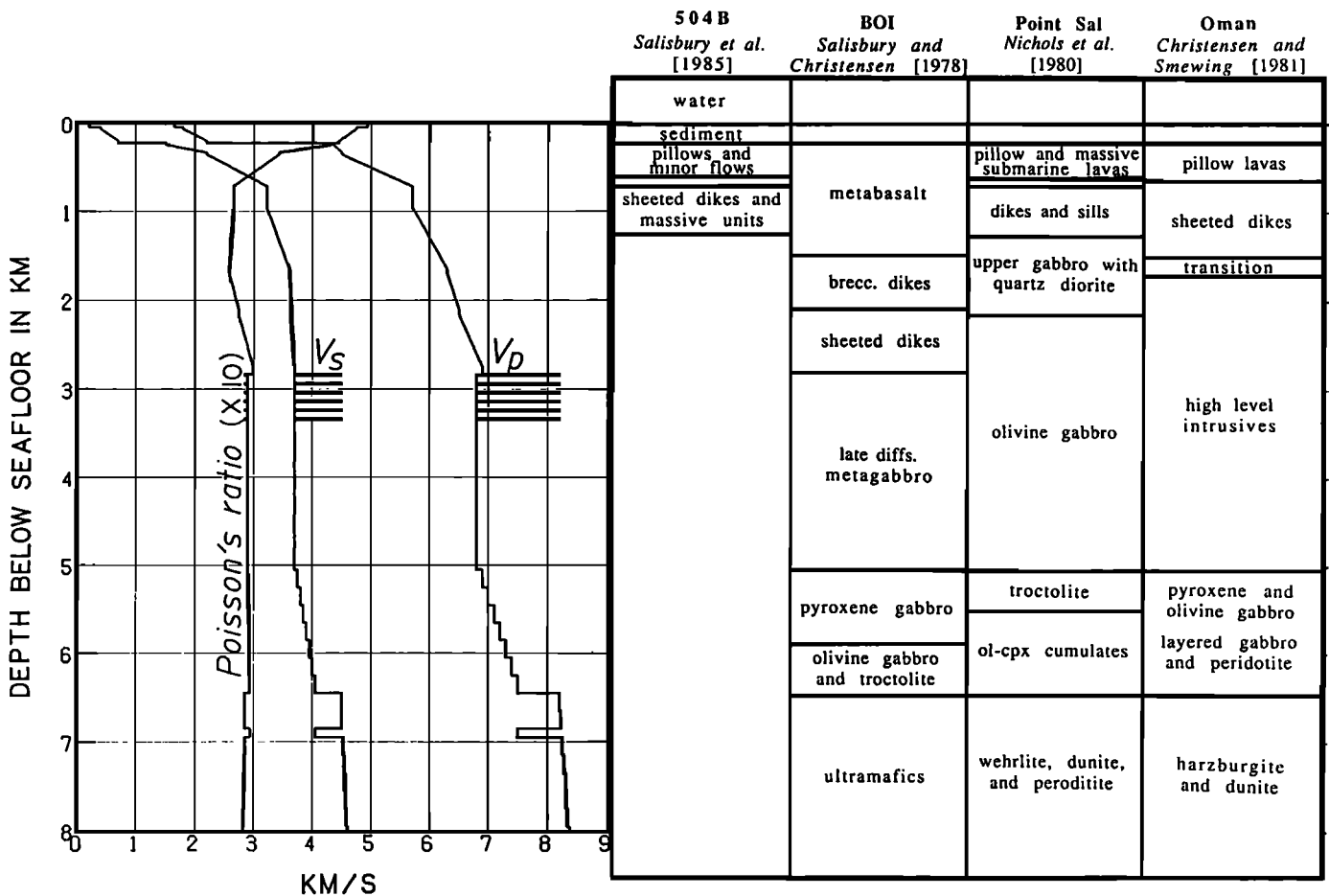


Fig. 13. Four lithological interpretations of ESP 1 based upon the measured velocities of specified samples from the four sources shown. 504B is an in situ sonic log of young Pacific crust. BOI, Point Sal, and Oman are laboratory measurements of samples from ophiolites which are believed to be former ocean crust which has been emplaced on land and has undergone varying degrees of distortion and metamorphism. The rock types shown are the terms used by the various authors. The interpretations based upon 504B, Point Sal, and Oman are fairly consistent with each other as well as with some independent considerations from the ESP model. The zero gradient zone between 0.7 and 1 km below the seafloor is not in the pillow layer. The high values of Poisson's ratio just below the seafloor are probably caused by the high porosity in the sediment and the pillow lavas, while the low Poisson's ratios below them are in layers of low porosity. The laminated structure starting at 2.8 km below the seafloor which may be ultramafic cumulates is well below the top of the gabbro layers. The interpretation based upon the BOI velocities, however, is very different from all of the others and violates all of the above arguments. The BOI velocities therefore are probably too high for the in situ pillow and dike basalts, and lithological interpretations of velocity profiles of ocean crust should be based on the other three data sets.

they are well below the basalt to gabbro horizon since there should be some gabbro above them from the solidification of the tops and sides of the magma chambers.

Based on all of the above arguments, the lithological interpretations derived from the Point Sal and Oman ophiolites and the 504B borehole are preferred over that from the BOI ophiolite (Figure 13). The interpretations using the 504B, Point Sal, and Oman velocities are very similar to each other, the zone of no gradient (0.7-0.9 km below the seafloor) is within the sheeted dikes, the area of low Poisson's ratio is below a zone of extensive cracking, and the thin, high-velocity layers (2.8-3.3 km depth) are below the top of the gabbro layer.

SUMMARY AND CONCLUSION

The general profile with depth of V_p , V_s , and Poisson's ratio for ESP 1 is much like most other ocean crustal profiles with a monotonically increasing V_p and V_s but a decreasing derivative of V_p and V_s with depth (Figure 4). Poisson's ratio is 0.5 at the top of the sediments and decreases with depth through the sediments and the uppermost 1 km of the igneous crust then increases again about 2 km below the base of the sediment. The total crustal thickness from the base of the sediments to the top of the mantle ($V_p > 8.0$ km/s) is 6.2 km. A lithological interpretation yields thicknesses for the major units as: pillows, 400-500 m; sheeted dikes, 600-900 m; upper and midlevel gabbro, 3.5-4.0 km; low-level gabbro with interbedded ultramafic cumulates, 1.5 km (Figure 13). Travel time modeling of four nearby sonobuoy records produced very similar profiles with the exception of one (sonobuoy 4) which was located near the Molokai Fracture Zone and had unusually low velocities for the upper 1.5 km of igneous crust.

The laminations at a depth of 2.8-3.3 km below the seafloor may be only occasionally present in the ocean crust and are probably irregular with substantial dips where present. These layers have probably been observed in some reflection profiles both near ESP 1 and in the North Atlantic. They are best explained as ultramafic cumulates that are the result of fractional crystallization of an upper level magma chamber.

Vertical anisotropy between depths of 0.7 and 2.0 km below the seafloor may be present and may account for the low values of Poisson's ratio, but the calculated values for Poisson's ratio are not extremely low and may be within the normal range of values for sheeted dike basalts and upper level gabbros.

The profiles of V_p , V_s , and Poisson's ratio with depth, combined with ophiolite studies and downhole logging measurements result in several possible lithological interpretations. Three of the four presented here are consistent with each other as well as with some logical constraints from the data (Figure 13). The fourth, which is from the most widely used data set for interpreting ocean crustal velocity profiles, has overly thick upper layers caused by altered basalts in the pillow and dike sections of the BOI ophiolite that have velocities that are about 1 km/s higher than the real crust. The preferred interpretation gives a total thickness for the basalt layers (pillows and dikes) of 1.0-1.5 km instead of the more commonly given values of 2-4 km.

Acknowledgments. I thank U. ten Brink, T. Brocher, T. Watts, P. Buhl, J. Mutter, and the multichannel seismic group at Lamont-Doherty Geological Observatory for providing the processed multichannel data. This work was inspired primarily by T. Brocher who also gave several careful reviews. L. N. Frazer and G. J. Fryer contributed their encouragement and support. Hawaii Institute of Geophysics contribution number 2423. NOARL contribution JA362:017:91.

REFERENCES

- Au, D., and R. M. Clowes, Shear-wave velocity structure of the oceanic lithosphere from ocean bottom seismometer studies, *Geophys. J. R. Astron. Soc.*, **77**, 105-123, 1984.
- Bratt, S. R., and G. M. Purdy, Structure and variability of oceanic crust on the flanks of the East Pacific Rise between 11° and 13° N, *J. Geophys. Res.*, **89**, 6111-6125, 1984.
- Brocher, T. M., and U. S. ten Brink, Variation in oceanic layer 2 elastic velocities near Hawaii and their correlation to lithospheric flexure, *J. Geophys. Res.*, **92**, 2647-2661, 1987.
- Brocher, T. M., J. A. Karson, and J. A. Collins, Seismic stratigraphy of the oceanic Moho based on ophiolite models, *Geology*, **13**, 62-65, 1985.
- Bunch, A. W. H., and B. L. N. Kennett, The crustal structure of the Reykjanes Ridge at 59° 30' N, *Geophys. J. R. Astron. Soc.*, **61**, 141-166, 1980.
- Casey, J. F., and J. A. Karson, Magma chamber profiles from the Bay of Islands ophiolite complex, *Nature*, **292**, 295-301, 1981.
- Casey, J. F., J. A. Karson, D. Elthon, E. Rosencrantz, and M. Titus, Reconstruction of the geometry of accretion during formation of the Bay of Islands ophiolite complex, *Tectonics*, **2**, 509-528, 1983.
- Cervený, V., I. A. Molotkov, and I. Psencik, *Ray Method in Seismology*, 214 pp., Univerzita Karlova, Praha, 1977.
- Chapman, C. H., and J. A. Orcutt, Least-squares fitting of marine seismic refraction data, *Geophys. J. R. Astron. Soc.*, **82**, 339-374, 1985.
- Christensen, N. I., Ophiolites, seismic velocities and oceanic crustal structure, *Tectonophysics*, **47**, 131-157, 1978.
- Christensen, N. I., and M. H. Salisbury, Lateral heterogeneity in the seismic structure of the oceanic crust inferred from velocity studies in the Bay of Islands ophiolite, Newfoundland, *Geophys. J. R. Astron. Soc.*, **68**, 675-688, 1982.
- Christensen, N. I., and J. D. Smewing, Geology and seismic structure of the northern section of the Oman ophiolite, *J. Geophys. Res.*, **86**, 2545-2555, 1981.
- Coleman, R. G., Tectonic setting for ophiolite obduction in Oman, *J. Geophys. Res.*, **86**, 2497-2508, 1981.
- Collins, J. A., T. M. Brocher, and J. A. Karson, Two-dimensional seismic reflection modeling of the inferred fossil oceanic crust/mantle transition in the Bay of Islands ophiolite, *J. Geophys. Res.*, **91**, 12520-12538, 1986.
- Collins, J. A., M. G. Purdy, and T. M. Brocher, Seismic velocity structure at deep sea drilling project site 504B, Panama Basin: Evidence for thin oceanic crust, *J. Geophys. Res.*, **94**, 9283-9302, 1989.
- Cormier, M., R. S. Detrick, and G. M. Purdy, Anomalous thin crust in oceanic fracture zones: New seismic constraints from the Kane fracture zone, *J. Geophys. Res.*, **89**, 10249-10266, 1984.
- Diebold, J. B., and P. L. Stoffa, The travelttime equation, tau-p mapping, and inversion of common midpoint data, *Geophysics*, **46**, 238-254, 1981.
- Defense Mapping Agency, Hawaiian Islands, Soundings in fathoms, scale 1:1,030,000, 19009, Washington, D. C., 1981.
- Juenebier, F. K., B. Lienert, R. Cessaro, P. Anderson, and S. Mallick, Controlled-source seismic experiment at hole 581C, *Proc. Ocean Drill. Program Initial Rep.*, **88**, 105-125, 1987.
- Engel, C. G., and A. E. J. Engel, Volcanic rocks dredged southwest of the Hawaiian Islands, *U.S. Geol. Surv. Prof. Pap.*, **550-D**, D104-D108, 1966.
- Fryer, G. J., D. J. Miller, and P. A. Berge, Seismic anisotropy and age-dependent structure of the upper oceanic crust, in *Evolution of Mid Ocean Ridges*, *Geophys. Monogr. Ser.*, **57**, edited by J. M. Sinton, 1-8, AGU, Washington, D. C., 1989.

- Green, C. H., Velocity determinations by means of reflection profiles, *Geophysics*, **3**, 295-305, 1938.
- Helmberger, D. V., and G. B. Morris, A travel time and amplitude interpretation of a marine refraction profile: Transformed shear waves, *Bull. Seismol. Soc. Am.*, **60**, 593-600, 1970.
- Hopson, C. A., R. G. Coleman, R. T. Gregory, J. S. Pallister, and E. H. Bailey, Geologic section through the Samail ophiolite and associated rocks along a Muscat-Ibra transect, southeastern Oman Mountains, *J. Geophys. Res.*, **86**, 2527-2544, 1981.
- Juteau, T., M. Beurrier, R. Dahl, and P. Nehlig, Segmentation at a fossil spreading axis: The plutonic sequence of the Wadi Haymiliyah area (Haylayn Block, Sumail Nappe, Oman), *Tectonophysics*, **151**, 167-197, 1988a.
- Juteau, T., M. Ernewein, I. Reuber, H. Whitechurch, and R. Dahl, Duality of magmatism in the plutonic sequence of the Sumail Nappe, Oman, *Tectonophysics*, **151**, 107-135, 1988b.
- Karson, J. A., J. A. Collins, and J. F. Casey, Geologic and seismic velocity structure of the crust/mantle transition in the Bay of Islands ophiolite complex, *J. Geophys. Res.*, **89**, 6126-6138, 1984.
- Kong, L., T. M. Brocher, and R. A. Stephen, Spreading rate independence of oceanic seismic layer 2, *Geophys. Res. Lett.*, **12**, 219-222, 1985.
- Lewis, B. T. R., and W. E. Snodgrass, Evidence for a low velocity layer at the base of the oceanic crust, *Nature*, **266**, 340-344, 1977.
- Lindwall, D. A., A two-dimensional seismic investigation of crustal structure under the Hawaiian islands near Oahu and Kauai, *J. Geophys. Res.*, **93**, 12107-12122, 1988.
- Little, S. A. and R. A. Stephen, Costa Rica rift borehole seismic experiment, deep sea drilling project hole 504B, leg 92, *Initial Rep. Deep Sea Drill. Proj.*, **83**, 517-528, 1985.
- Mallick, S., and L. N. Frazer, Practical aspects of reflectivity modeling, *Geophysics*, **52**, 1355-1364, 1987.
- Mallick, S., and L. N. Frazer, Rapid computation of multi-offset VSP synthetic seismograms for layered media, *Geophysics*, **53**, 479-491, 1988.
- McCarthy, J., and J. C. Mutter, Relict magma chamber structures preserved within the Mesozoic North Atlantic crust, *Eos Trans. AGU*, **67**, 1083, 1986.
- McCarthy, J., J. C. Mutter, J. L. Morton, N. H. Sleep, and G. A. Thompson, Relict magma chamber structures preserved within the Mesozoic North Atlantic crust?, *Geol. Soc. Am. Bull.*, **100**, 1423-1436, 1988.
- Mutter, J. C., and NAT Study Group, Multichannel seismic images of the oceanic crust's internal structure: Evidence for a magma chamber beneath the Mesozoic mid-Atlantic Ridge, *Geology*, **13**, 692-632, 1985.
- NAT Study Group, North Atlantic transect: A wide-aperture, two-ship multichannel seismic investigation of the oceanic crust, *J. Geophys. Res.*, **90**, 10321-10341, 1985.
- Nehlig, P., and T. Juteau, Flow porosities, permeabilities and preliminary data on fluid inclusions and fossil thermal gradients in the crustal sequence of the Sumail ophiolite (Oman), *Tectonophysics*, **151**, 199-221, 1988.
- Newmark, R. L., R. N. Anderson, D. Moos, and M. D. Zoback, Structure, porosity and stress regime of the upper oceanic crust: Sonic and ultrasonic logging of DSDP hole 504B, *Tectonophysics*, **118**, 1-42, 1985a.
- Newmark, R. L., R. N. Anderson, D. Moos, and M. D. Zoback, Sonic and ultrasonic logging of hole 504B and its implications for the structure, porosity, and stress regime of the upper 1 km of the oceanic crust, *Initial Rep. Deep Sea Drill. Proj.*, **83**, 479-510, 1985b.
- Nichols, J., N. Warren, B. P. Luyendyk, and P. Spudich, Seismic velocity structure of the ophiolite at Point Sal, southern California, determined from laboratory measurements, *Geophys. J. R. Astron. Soc.*, **63**, 165-185, 1980.
- Nicolas, A., I. Reuber, and K. Benn, A new magma chamber model based on structural studies in the Oman ophiolite, *Tectonophysics*, **151**, 87-105, 1988.
- Purdy, G. M., The seismic structure of 140 Myr old crust in the western central Atlantic Ocean, *Geophys. J. R. Astron. Soc.*, **72**, 115-137, 1983.
- Purdy, G. M., New observations of the shallow seismic structure of young oceanic crust, *J. Geophys. Res.*, **92**, 9351-9362, 1987.
- Reuber, I., Complexity of the crustal sequence in the northern Oman ophiolite (Fizh and southern Aswad blocks): The effect of early slicing?, *Tectonophysics*, **151**, 137-165, 1988.
- Rohr, K., Variations of the amplitudes of reflections from old oceanic basement in the North Atlantic, *J. Geophys. Res.*, **92**, 10581-10594, 1987.
- Sager, W. W., and M. S. Pringle, Paleomagnetic constraints on the origin and evolution of the Muscat and South Hawaiian seamounts, central Pacific Ocean, in *Seamounts, Islands, and Atolls, Geophys. Monogr. Ser.*, vol. 43, edited by B. Keating, P. Fryer, R. Batiza, and G. Boehlert, pp. 133-162, AGU, Washington, D.C., 1987.
- Salisbury, M. H., Investigations of seismic velocities in the Bay of Islands, Newfoundland ophiolite complex for comparison with oceanic seismic structure, Ph.D. thesis, 197pp., Univ. of Wash., Seattle, 1974.
- Salisbury, M. H., and N. I. Christensen, The seismic velocity structure of a traverse through the Bay of Islands ophiolite complex, Newfoundland, an exposure of oceanic crust and upper mantle, *J. Geophys. Res.*, **83**, 805-817, 1978.
- Salisbury, M. H., N. I. Christensen, K. Becker, and D. Moos, The velocity structure of layer 2 at deep sea drilling project site 504 from logging and laboratory experiments, in *Initial Rep. Deep Sea Drill. Proj.*, **83**, 529-539, 1985.
- Spudich, P., and J. Orcutt, Petrology and porosity of an oceanic crustal site: Results from wave form modeling of seismic refraction data, *J. Geophys. Res.*, **85**, 1409-1433, 1980a.
- Spudich, P., and J. Orcutt, A new look at the seismic velocity structure of the oceanic crust, *Rev. Geophys. Space Phys.*, **18**, 627-645, 1980b.
- Spudich, P., and J. Orcutt, Correction to "Petrology and Porosity of an Oceanic Crustal Site: Results From Wave Form Modeling of Seismic Refraction Data" by Paul Spudich and John Orcutt, *J. Geophys. Res.*, **92**, 11669, 1987.
- Stephen, R., Seismic anisotropy in the upper oceanic crust, *J. Geophys. Res.*, **90**, 11383-11396, 1985.
- Stoffa, P. L., and P. Buhl, Two-ship multichannel seismic experiments for deep crustal studies: Expanded spread and constant offset profiles, *J. Geophys. Res.*, **84**, 7645-7660, 1979.
- Stoffa, P. L., J. B. Diebold, and P. Buhl, Velocity analysis for wide aperture seismic data, *Geophys. Prospect.*, **30**, 25-57, 1982.
- ten Brink, U. S., and T. M. Brocher, Multichannel seismic evidence for a subcrustal intrusive complex under Oahu and a model for Hawaiian volcanism, *J. Geophys. Res.*, **92**, 13687-13707, 1987.
- ten Brink, U. S., and T. M. Brocher, Multichannel seismic evidence for variation in crustal thickness across the Molokai fracture zone in the mid-Pacific, *J. Geophys. Res.*, **93**, 1119-1130, 1988.
- Torresan, M. E., A. N. Shor, J. B. Wilson, and J. Campbell, Cruise Report, Hawaiian GLORIA Leg 5, *U.S. Geol. Surv. Open File Rep.* 89-198, 1989.
- Watts, A. B., J. H. Bodine, and M. S. Steckler, Observations of flexure and the state of stress in the oceanic lithosphere, *J. Geophys. Res.*, **85**, 6369-6376, 1980.
- Watts, A. B., U. S. ten Brink, P. Buhl, and T. M. Brocher, A multichannel seismic study of lithospheric flexure across the Hawaiian-Emperor seamount chain, *Nature*, **315**, 105-111, 1985.
- White, R. S., and G. M. Purdy, Crustal velocity structure on the flanks of the mid-Atlantic ridge at 24°N, *Geophys. J. R. Astron. Soc.*, **75**, 361-385, 1983.
- White, R. S., R. S. Detrick, M. C. Sinha, and M. H. Cormier, Anomalous seismic crustal structure of oceanic fracture zones, *Geophys. J. R. Astron. Soc.*, **79**, 779-798, 1984.

D. A. Lindwall, Naval Oceanographic and Atmospheric Research Laboratory, Code 362, Stennis Space Center, MS 39529.

(Received June 23, 1989;
revised December 27, 1990;
accepted May 7, 1990.)